Limitations of the dual voltage clamp method in assaying conductance and kinetics of gap junction channels

Ronald Wilders and Habo J. Jongsma
Department of Physiology, University of Amsterdam, 1105 AZ Amsterdam, The Netherlands

ABSTRACT The electrical properties of gap junctions in cell pairs are usually studied by means of the dual voltage clamp method. The voltage across the junctional channels, however, cannot be controlled adequately due to an artificial resistance and a natural resistance, both connected in series with the gap junction. The access resistances to the cell interior of the recording pipettes make up the artificial resistance. The natural resistance consists of the cytoplasmic access resistances to the tightly packed gap junction channels in both cells. A mathematical model was constructed to calculate the actual voltage across each gap junction channel. The stochastic open-close kinetics of the individual channels were incorporated into this model. It is concluded that even in the ideal case of complete compensation of pipette series resistance, the number of channels comprised in the gap junction may be largely underestimated. Furthermore, normalized steady-state junctional conductance may be largely overestimated, so that transjunctional voltage dependence is easily masked. The model is used to discuss conclusions drawn from dual voltage clamp experiments and offers alternative explanations for various experimental observations.

INTRODUCTION

The dual voltage clamp method is the common method to assay the electrical properties of gap junctions, such as junctional conductance and transjunctional voltage dependence. In the first applications, each cell of a cell pair was impaled with two microelectrodes, allowing independent current injection and voltage control (Harris et al., 1981; Spray et al., 1981). Presently, the most widely used dual voltage clamp method is the double whole cell voltage clamp technique with one suction pipette on each cell of a cell pair (Neyton and Trautmann, 1985; White et al., 1985; Weingart, 1986). The pipette solution is brought into continuity with the cytoplasm by rupturing, with gentle suction, the membrane under the tip of the pipette. The small tip becomes partially clogged with fragments of the broken membrane patch, resulting in an access resistance to the cell interior that is considerably larger than the resistance of the pipette alone (Table 1). This pipette series resistance has been reported to increase during an experiment, probably due to an increase in pipette clogging or a slight drift of the cell surface away from the pipette (Noma and Tsuboi, 1987; Giaume, 1991; Rook, 1991; Takens-Kwak et al., 1992). Simple models to calculate the errors introduced by the pipette series resistance have been constructed (Weingart, 1986; Giaume, 1991), showing that large errors are easily attained.

One may try to compensate for the pipette series resistance by means of an electronic series resistance compensation circuit. Of course, a reduction in series resistance is achieved, but the error introduced by incomplete compensation can be appreciable (Moreno et al., 1991*a*). Also, one may try to correct for the pipette series resistance by means of correction formulas (Neyton and Trautmann, 1985; Rook et al., 1988; Giaume, 1991). These formulas can only be used if reliable estimates of the pipette series resistance are available. Different estimation methods, however, may yield markedly different estimates (Takens-Kwak, B. R., unpublished observations). To avoid the problems introduced by pipette series resistance, some investigators modified the preparation (Noma and Tsuboi, 1987), whereas others modified the clamp protocol, using combinations of voltage clamp and current clamp (Wittenberg et al., 1986; Chanson et al., 1988).

Table 2 summarizes the results from experiments on gap junctions in pairs of mammalian cardiac myocytes. Neonatal cell pairs may exhibit transjunctional voltage dependence, i.e., transjunctional voltage clamp steps may induce junctional currents that diminish during the step. This phenomenon does not occur until transjunctional voltage exceeds 50–60 mV (Rook et al., 1988; Veenstra, 1991*a*), explaining why Burt and Spray (1988) did not observe it (Table 2). The differences in transjunctional voltage dependence between neonatal and adult pairs of mammalian cardiac myocytes may be explained by the hypothesis that relative amounts of distinct channel forming proteins (connexins), possessing different gating properties, change during development (Spray and Burt, 1990). This hypothesis, however, does not explain why in neonatal cell pairs transjunctional voltage dependence is only observed if junctional conductance is low (Table 2).

Moreno et al. (1991*b*) pointed out that high pipette series resistances may lead to an apparent disappearance of transjunctional voltage dependence. Simple calculations show that this effect is not large enough to explain the disappearance of transjunctional voltage dependence observed in our laboratory by Rook et al. (1988) and Takens-Kwak et al. (1992). Rook et al. (1988, 1990) argued that the cytoplasmic potential drop, resulting from the access resistance to the narrow, tightly packed junc-

Address correspondence to Dr. Wilders.

0006-3495/92/10/942/12 $2.00

tional channels, might be so large that the voltage across the channels was considerably less than the applied voltage, and voltage dependence was masked. Following Hille (1968, 1984), access resistance was included in calculations of the resistance of a single junctional channel based on the geometry of the channel (Burt and Spray, 1988; Rüdisüli and Weingart, 1989, 1991). In these calculations, access resistance amounts to <10% of single channel resistance. This, however, does not imply that the cytoplasmic access resistance is <10% of the apparent junctional resistance in moderate-sized gap junctions, due to the tight packing of the junctional channels in hexagonal arrays, as observed in gap junctions of liver (Makowski et al., 1984) and heart (Manjunath and Page, 1985). Simple models, yielding rough estimates of the errors introduced by the cytoplasmic access resistance, were constructed (Jongsma et al., 1990, 1991). Model results indicated that cytoplasmic access resistance might play an important role.

To test our hypothesis that inadequate control of the voltage across the junctional channels may explain the observation that large gap junctions between mammalian cardiac myocytes do not exhibit transjunctional voltage dependence (Jongsma and Wilders, 1992), we constructed a mathematical model incorporating pipette series resistance, cytoplasmic access resistance, and time- and voltage-dependent gating of the junctional channels. The geometry of the channels as well as their gating behavior were modeled according to the available experimental data.

GLOSSARY

Symbols

α	rate constant of channel openings
β	rate constant of channel closures
γ	pore conductance
ΔV_{app}	applied voltage or apparent transjunctional voltage
$\Delta V_{channels}$	voltage across the junctional channels
ΔV_{cyt}	cytoplasmic potential drop
ΔV_j	transjunctional voltage
ΔV_m (ΔV_n)	voltage across channel m (n)
ΔV_0	voltage at which α equals β
λ	rate at which α equals β
ρ	cytoplasmic resistivity
τ	time constant of channel gating
A_α (A_β)	voltage sensitivity of rate constant α (β)
d_c	channel diameter
d_{cell}	cell diameter
d_{gj}	gap junction diameter
d_{hex}	lattice constant
g_j	junctional conductance
$g_{j,0}$ ($g_{j,\infty}$)	instantaneous (steady-state) junctional conductance
G_j	normalized junctional conductance
$G_{j,\infty}$	normalized steady-state junctional conductance
i_m (i_n)	current through channel m (n)
I_j	junctional current
$I_{j,0}$ ($I_{j,\infty}$)	instantaneous (steady-state) junctional current
l_{cell}	length of cell
l_{gj}	length of gap junction
N	number of channels comprised in the gap junction
P_o	single channel open probability
r	distance from center of channel mouth
r_c	channel radius
$r_{m,n}$	center-to-center spacing of channels m and n
$R_{acc,channel}$	cytoplasmic access resistance to the mouth of a single channel
$R_{acc,shell}$	cytoplasmic access resistance to a hemispherical shell over the mouth of a single channel
$R_{channels}$	resistance of the junctional channels
$R_{cyt,A}$ ($R_{cyt,B}$)	cytoplasmic access resistance in cell A (B)
R_j	junctional resistance
$R_{m,A}$ ($R_{m,B}$)	membrane resistance of cell A (B)
$R_{m,n}$	cytoplasmic access resistance of channel n at the mouth of channel m
R_{pip}	average of $R_{pip,A}$ and $R_{pip,B}$
$R_{pip,A}$ ($R_{pip,B}$)	access resistance to the cell interior of the pipette on cell A (B)
T_c (T_o)	single channel closed (open) time
V_A (V_B)	potential at which cell A (B) is clamped
$V_{m,A}$ ($V_{m,B}$)	membrane potential of cell A (B)

Constants

$\gamma = 50$ pS
$\Delta V_0 = 78$ mV
$\lambda = 0.80\ s^{-1}$
$\rho = 330\ \Omega cm$
$A_\alpha = 0.040\ mV^{-1}$
$A_\beta = 0.019\ mV^{-1}$
$d_c = 1.8$ nm
$d_{cell} = 26\ \mu m$
$d_{hex} = 9.5$ nm
$l_{cell} = 26\ \mu m$
$l_{gj} = 15.4$ nm
$r_c = 0.9$ nm

MATERIALS AND METHODS

Experiments

Experimental results presented in Fig. 6 *A* were obtained in our laboratory by M. B. Rook, H. J. Jongsma, and A. C. G. van Ginneken, whereas those presented in Fig. 9 *A* were obtained by B. R. Takens-Kwak, H. J. Jongsma, and A. C. G. van Ginneken. Their experimental methods have been described in detail elsewhere (Rook et al., 1988; Takens-Kwak et al., 1992).

Numerical computations

A finite difference representation of Laplace's potential equation (Eq. 2) and associated boundary conditions were constructed according to Forsythe and Wasow (1960). The resulting large system of simultaneous algebraic equations of five point molecule form was solved numerically by means of NAG algorithm (D03EBF; Numerical Algorithms Group, Ltd., England) on a computer (model 3090-600J/6VF; International Business Machines Corporation, Armonk, NY).

The model described by Eqs. 8–18 was translated into a FORTRAN computer program, in which the $N \times N$ system of linear equations

resulting from Eq. 9 was solved for ΔV_m, $m = 1, \ldots, N$, by means of LU decomposition. For small N, the program was run on a computer (models PDP 11/73 or VAX 4000-300; Digital Equipment Corporation, Maynard, MA). For large N, an IBM ES/9000-720, equipped with vector facilities, was used.

MATHEMATICAL MODEL

Geometry

A cell pair is modeled as two right cylindrical volumes of the same size, connected by a gap junction that has a right cylindrical appearance as well (Fig. 1 *A*). The junctional channels are arranged in a lattice of regular hexagons, consisting of a central hexagon surrounded by a number of concentric annuli of hexagons (Fig. 1 *B*). The kth annulus comprises $6k$ channels. As a consequence, the number of channels, N, is related to the gap junction diameter through

$$N = 0.25 + 0.75(d_{gj}/d_{hex})^2. \quad (1)$$

Each junctional channel is modeled as an aqueous right cylindrical pore (Fig. 1, *B* and *C*). The resistivity of the fluid filling the pore is assumed to be the same as the cytoplasmic resistivity.

Revel and Karnovsky (1967) reported that gap junctions in mouse heart were arranged in hexagonal arrays with lattice constants of 9.0–9.5 nm. Gap junctions between rat ventricular and mouse atrial myocardial cells contain approximately hexagonally arranged channels, with surface densities of $12{,}900 \pm 700\ \mu m^{-2}$ (mean ± SD, $n = 6$) and $16{,}900 \pm 1{,}400\ \mu m^{-2}$ (mean ± SD, $n = 3$), respectively (Manjunath and Page, 1985), corresponding with lattice constants of 9.5 and 8.3 nm, respectively. In our laboratory, in rat cardiac gap junctions a surface density of $\sim 12{,}000\ \mu m^{-2}$ was observed (Masson-Pévet, M. A., unpublished data), yielding a lattice constant of ~9.8 nm. Slightly smaller lattice constants were found in liver gap junctions. The lattice constant was reported to be ~8.5 nm in rat liver (Zampighi and Unwin, 1979), whereas values ranging from 7.4 to 8.8 nm were observed in mouse liver (Makowski et al., 1984). As an average of the data on heart gap junctions, we set the lattice constant to 9.5 nm in our model.

The "limiting diameter" of junctional channels between mammalian cells lies between 1.6 and 2.0 nm (Schwarzmann et al., 1981). Zampighi and Unwin (1979) observed a "total thickness" of rat liver gap junctions of ~15 nm. According to Makowski et al. (1984), mouse liver gap junctions contain right cylindrical pores of ~15 nm in length. In a recent study, a value of 15.4 ± 1.5 nm (mean ± SD, $n = 13$) was obtained for the "total width" of gap junctions between rabbit cardiac myocytes (de Mazière et al., 1992). In agreement with these data, we set the diameter and length of the junctional channels, d_c and l_{gj} in Fig. 1, to 1.8 and 15.4 nm, respectively, in our model.

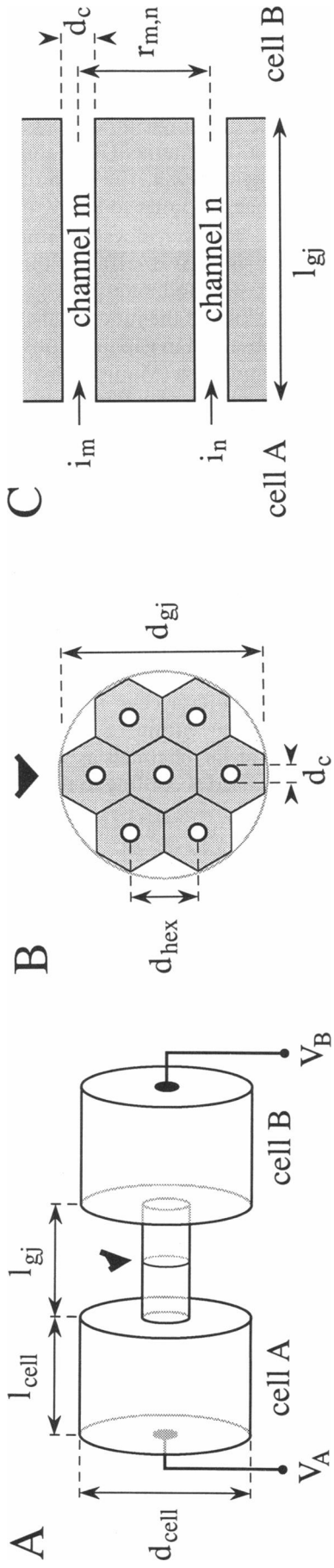

FIGURE 1 (*A*) Model of a cell pair connected by a gap junction. The cells as well as the gap junction are represented by a right cylindrical volume. The diameter (length) of both cells is d_{cell} (l_{cell}), the gap junction length is l_{gj}, and the potential at which cell A (cell B) is clamped is V_A (V_B). (*B*) Transverse-section of the model gap junction. The gap junction consists of a number of right cylindrical channels arranged in a lattice of regular hexagons. The diameter of the gap junction (a gap junction channel) is d_{gj} (d_c), and the lattice constant is d_{hex}. (*C*) Longitudinal section through channels m and n of the model gap junction. The current flowing from cell A to cell B through channel m (n) is i_m (i_n), and the center-to-center spacing of channels m and n is $r_{m,n}$.

Equivalent resistive circuit

Fig. 2 shows the equivalent resistive circuit for the cell pair of Fig. 1 *A*. For the sake of simplicity, we left out the seal resistance of the suction pipettes. This resistance is so large, typical values being 5–50 GΩ (Veenstra and DeHaan, 1988), >10 GΩ (Rook et al., 1988, 1990), and 10–50 GΩ (Takens-Kwak et al., 1992), that errors arising from seal leakage currents may be neglected. Also, we did not incorporate a resistive path between the junctional channels and the intercellular cleft. In cardiac cells, leakage currents at that point, if any, must be small, because junctional conductance is not dependent on membrane potential (Weingart, 1986; Veenstra and DeHaan, 1988).

The membrane resistance of neonatal heart cells is typically on the order of 2–5 GΩ (Burt and Spray, 1988; Rook et al., 1988; Veenstra and DeHaan, 1988). Consequently, the potential drop introduced by membrane current is <1% (<5%) of the applied voltage if pipette series resistance is <20 MΩ (<100 MΩ). Membrane resistance of adult rat ventricular cells, on the other hand, may be as low as 10–100 MΩ (Wittenberg et al., 1986). Junctional resistance between adult ventricular cells, however, is also low (Table 2), the ratio between membrane resistance and junctional resistance being 10:100 (Kameyama, 1983; Weingart, 1986; Wittenberg et al., 1986). Consequently, the potential drop introduced by membrane current is small compared with that introduced by junctional current. Thus, for our purposes, membrane resistance may be left out of the model. What remains is a junctional resistance connected in series, on both sides, with a pipette resistance. The only current flowing in this simplified circuit is the junctional current. Without loss of generality, we assume $R_{cyt,A} = R_{cyt,B}$, $R_{pip,A} = R_{pip,B} = R_{pip}$, and $V_B = -V_A$, $V_A \geq 0$. Then, for reasons of symmetry, the potential halfway through the junctional channels always equals 0.

Monochannel gap junction

Let us consider the case $N = 1$ to start with. The gap junction then comprises only one channel, and the geometrical model (Fig. 1 *A*) displays rotational symmetry. As a consequence, using cylindrical coordinates (r, ϑ, z), Laplace's potential equation reduces to

$$\frac{\partial^2 V}{\partial r^2} + \frac{1}{r}\frac{\partial V}{\partial r} + \frac{\partial^2 V}{\partial z^2} = 0 \qquad (2)$$

in two dimensions. With the boundary conditions that (*a*) the cell membrane near the pipette has a constant potential of 100 arbitrary units, (*b*) no current crosses the remaining part of the nonjunctional membrane or the channel wall, and (*c*) the potential equals 0 halfway through the channel (Fig. 3 *A*), Eq. 2 was solved numerically. The resulting equipotential planes are depicted in Fig. 3 *B*. The position and shape of these planes hardly depend on the cell dimensions, provided that the dimensions of the channel are small compared with the cell dimensions. At the mouth of the channel, the potential has dropped to a nearly constant value of ~91, the cytoplasmic potential drop, ΔV_{cyt}, being ~9%. The black lines in Fig. 3 *C* show ΔV_{cyt} as a function of the radial distance from the center of the channel mouth. Note that, thus far, these results do not depend on the pore conductance γ nor on the cytoplasmic resistivity ρ, related to each other through

$$\gamma = \pi r_c^2/(\rho l_{gj}). \qquad (3)$$

If $N \geq 2$, then rotational symmetry is no longer present and Laplace's full equation in three dimensions has to be

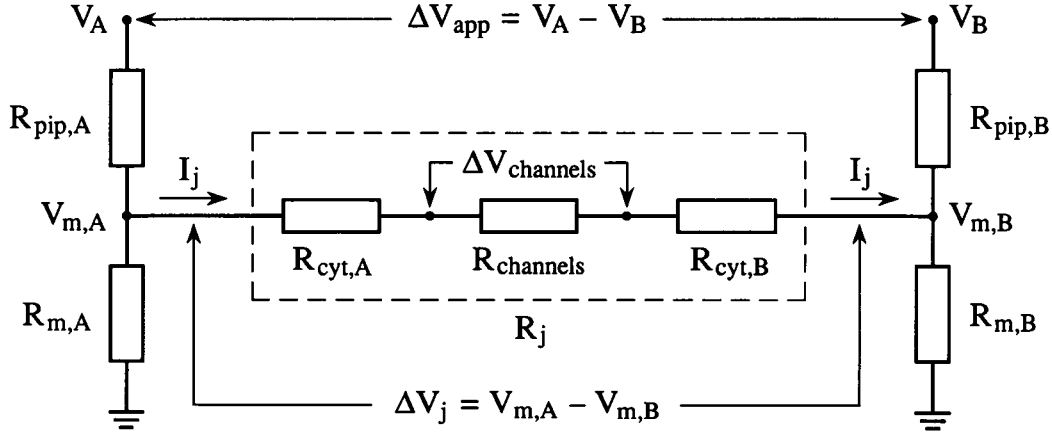

FIGURE 2 Equivalent resistive circuit for the double whole-cell voltage clamp configuration as shown in Fig. 1 *A*. The junctional resistance, R_j, consists of the resistance formed by N parallel junctional channels with pore conductance γ, $R_{channels}$, and the cytoplasmic access resistances to these channels in cell A and cell B, $R_{cyt,A}$ and $R_{cyt,B}$. The applied voltage, ΔV_{app}, is the difference of the potentials in the suction pipettes placed on cell A and cell B, V_A, and V_B. The transjunctional voltage, ΔV_j, is the difference of the membrane potentials of cell A and cell B, $V_{m,A}$, and $V_{m,B}$. The membrane resistance of cell A (cell B) is $R_{m,A}$ ($R_{m,B}$), and the access resistance to the cell interior of the suction pipette placed on cell A (cell B) is $R_{pip,A}$ ($R_{pip,B}$). The junctional current is I_j, and the voltage across the junctional channels is $\Delta V_{channels}$.

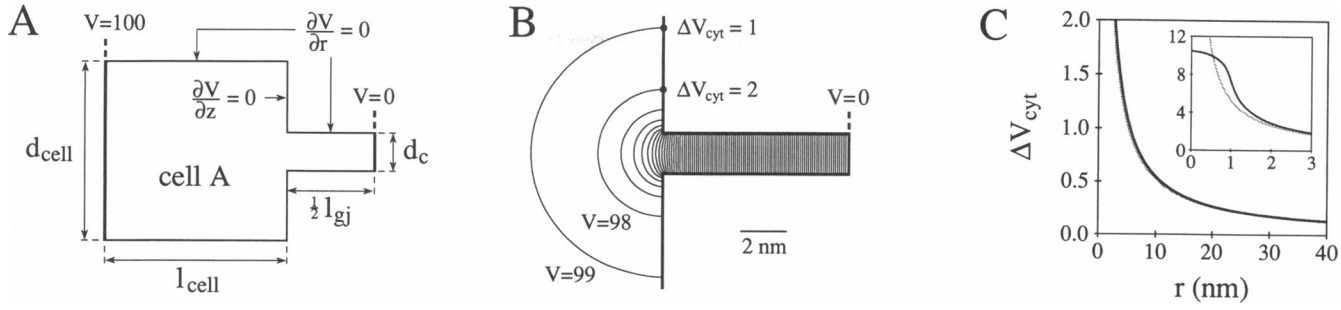

FIGURE 3 (*A*) Longitudinal section through cell A and half of a one-channel gap junction showing the boundary conditions for the calculation of equipotential planes: on the left side the potential, *V*, equals 100 (arbitrary units) and on the right side *V* equals 0. At the remaining parts of the boundary the normal derivative equals 0. The diameter (length) of the cell is d_{cell} (l_{cell}), and the diameter (length) of the gap junction channel is d_c (l_{gj}). (*B*) Equipotential planes, plotted 1 arbitrary unit apart. $d_{cell} = l_{cell} = 26$ μm, $d_c = 1.8$ nm, and $l_{gj} = 15.4$ nm. (*C*) Cytoplasmic potential drop, ΔV_{cyt}, as a function of the distance from the channel mouth, *r*, according to the equipotential planes of *B* (*black lines*) or Eqs. 3–5 (*grey lines*).

solved, but this seems an unfeasible task, especially for large *N*. Fortunately, a method that can be extended to the $N \geq 2$ case without difficulties and yields good approximations to the data of Fig. 3, *B* and *C*, can be obtained as follows. If the mouth of the channel is an equipotential plane, the cytoplasmic access resistance to the channel can be calculated exactly, yielding

$$R_{acc,channel} = \rho/(4r_c) \quad (4)$$

(Hall, 1975; Hille, 1984), whereas the cytoplasmic access resistance up to a hemispherical shell over the channel mouth of radius $r > r_c$ can be approximated by

$$R_{acc,shell} = \rho/(2\pi r) \quad (5)$$

(Hille, 1968, 1984; Hall, 1975). According to Eqs. 3 and 4, the potential at the mouth of the channel, for the case presented in Fig. 3 *A*, is 91.6 (arbitrary units). Next, ΔV_{cyt} can be calculated from Eqs. 3 and 5 (Fig. 3 *C*, grey lines). Note that, again, these results do not depend on γ or ρ.

Single channel conductance

Single gap junction channels obey Ohm's law with mean conductance values at ~21°C of 43 pS (Rook et al., 1988; Rook, 1991), 53 pS (Burt and Spray, 1988) and 42–44 pS (Takens-Kwak et al., 1992) in pairs of neonatal rat heart cells, and 37 pS in pairs of adult guinea pig ventricular cells (Rüdisüli and Weingart, 1989, 1991). These values include, of course, cytoplasmic access resistance. We set the model pore conductance, excluding cytoplasmic access resistance, to 50 pS, yielding a single channel conductance, calculated from Eqs. 3 and 4, of ~46 pS. According to Eq. 3, the 50 pS pore conductance involves a cytoplasmic resistivity of 330 Ωcm. This is consistent with the experimental value of 230 Ωcm in mammalian ventricle at 37°C (Chapman and Fry, 1978): with the Q_{10} of 1.3 for aqueous diffusion (Hille, 1984), it is 350 Ωcm at 21°C.

Multichannel gap junction

Let us now consider the case $N \geq 2$. The center-to-center spacing of channels *m* and *n* (Fig. 1 *C*) cannot be less than the lattice constant (Fig. 1 *B*). Therefore, according to Fig. 3 *C*, Eq. 5 can be used to approximate the cytoplasmic access resistance of channel *n* at the mouth of channel *m*, $R_{m,n}$. Thus, we have

$$R_{m,n} = \rho/(2\pi r_{m,n}). \quad (6)$$

The voltage across channel *m* will equal the applied voltage minus (*a*) the potential drop across the two pipettes, (*b*) the potential drop across the access resistance of channel *m* in both cells, and (*c*) the potential drop across the access resistances of the remaining channels at the mouth of channel *m* in both cells. Thus, we have

$$\Delta V_m = \Delta V_{app} - 2I_j R_{pip} - 2i_m R_{acc,channel} - \sum_{n \neq m} 2i_n R_{m,n} \quad (7)$$

for each channel *m*, $m = 1, \ldots, N$, where, obviously,

$$I_j = \sum_{n=1}^{N} i_n. \quad (8)$$

Combining Eqs. 3, 4, 6, 7, and 8, we arrive at

$$\left(1 + \frac{\pi r_c}{2l_{gj}} + 2\gamma R_{pip}\right)\Delta V_m + \sum_{n \neq m} \left(\frac{r_c^2}{l_{gj} r_{m,n}} + 2\gamma R_{pip}\right)\Delta V_n = \Delta V_{app}, \quad m = 1, \ldots, N. \quad (9)$$

Eq. 9 defines a system of *N* simultaneous linear equations that can be readily solved to give the *N* unknown voltages ΔV_m, $m = 1, \ldots, N$. Next, i_m, $m = 1, \ldots, N$, can be calculated from

$$i_m = \gamma \Delta V_m. \quad (10)$$

Of course, ΔV_m, $m = 1, \ldots, N$, need not be equal. If, e.g., $N \approx 2{,}000$ and $R_{pip} = 0$, they range from ~50% of ΔV_{app} for the central channel to ~63% of ΔV_{app} for the

peripheral channels. For the sake of simplicity, however, we will refer to

$$\Delta V_{\text{channels}} = \frac{1}{N} \sum_{m=1}^{N} \Delta V_m \tag{11}$$

as the voltage across the channels of the gap junction under consideration.

Gating of junctional channels

To model the time dependence of junctional currents, data on the stochastic open-close kinetics of single junctional channels are needed. Single channel data obtained after application of uncoupling agents are not useful, because these agents affect the single channel open probability (Burt and Spray, 1988; Rüdisüli and Weingart, 1989, 1991; Takens-Kwak et al., 1992). Fortunately, the data obtained by Rook et al. (1988) in newly formed pairs of neonatal rat heart cells under control conditions provide enough information to reconstruct the gating mechanism. At a transjunctional voltage of 50 mV, they observed average open and closed times of 2,283 ms (n = 9) and 418 ms (n = 12), respectively. At 100 mV, these figures were 965 ms (n = 25) and 3,035 ms (n = 36), respectively. The distributions of open as well as closed times had a negative exponential appearance. So, the open-close kinetics can be modeled satisfactorily with a single gate displaying first order kinetics (Colquhoun and Hawkes, 1983). Following Harris et al. (1981), we define the rate constants α and β by

$$\alpha = \lambda \exp[-A_\alpha(\Delta V - \Delta V_0)] \tag{12}$$

and

$$\beta = \lambda \exp[A_\beta(\Delta V - \Delta V_0)] \tag{13}$$

where the voltage across the channel is ΔV, the voltage sensitivity of α (β) is A_α (A_β), and the rate (voltage) at which α equals β is λ (ΔV_0). Keeping in mind that the average open (closed) time equals β^{-1} (α^{-1}) (Colquhoun and Hawkes, 1983) and that the voltage across a single open channel is ~91% of the transjunctional voltage (Fig. 3 *B*), the parameters λ, ΔV_0, A_α, and A_β can be derived from the above mentioned open and closed times, resulting in $\lambda = 0.80\ s^{-1}$, $\Delta V_0 = 78$ mV, $A_\alpha = 0.040$ mV^{-1}, and $A_\beta = 0.019\ mV^{-1}$. Fig. 4 *A* shows α and β as a function of the voltage across the channel. The corresponding open probability function is shown in Fig. 4 *B*, together with the time constant. Particular open times, T_o, and closed times, T_c, can be obtained by drawing a random number, x, from the uniform distribution on [0, 1] and calculating T_o and T_c from

$$T_o = (-\log x)/\beta \tag{14}$$

and

$$T_c = (-\log x)/\alpha \tag{15}$$

(Clay and DeFelice, 1983).

Voltage clamp steps

Eqs. 14 and 15, together with Eqs. 8–10, can be used to calculate the junctional current in response to a voltage clamp step in ΔV_{app} from 0 to any positive value. At $\Delta V_{app} = 0$, the voltage across each channel equals 0, and so we have $P_o \approx 1$ for each channel (Fig. 4 *B*). Therefore, we assume all channels to be open at the beginning of the step. A stochastic process of channel closures, and subsequent openings, is initiated by the voltage clamp step. This process is modeled as follows. Starting with all channels in the open state, the instantaneous I_j is calculated from Eqs. 8–10. Next, Eq. 15 is used to calculate the time at which the first channel closes, resulting in a modification of the configuration of open channels. Therefore, I_j is recalculated, using modified forms of Eqs. 8–10. Next Eqs. 14 and 15 are used to calculate the time at which the next channel opening or closure takes place. These calculations are repeated until I_j has reached a quasi-steady-state value, $I_{j,\infty}$. The (apparent) junctional conductance is calculated from

$$g_j = I_j/\Delta V_{app}. \tag{16}$$

The normalized (quasi) steady-state conductance is calculated from

$$G_{j,\infty} = g_{j,\infty}/g_{j,0} \tag{17}$$

or equivalently,

$$G_{j,\infty} = I_{j,\infty}/I_{j,0}. \tag{18}$$

RESULTS AND DISCUSSION

Instantaneous junctional conductance

To start with, we calculated the actual voltage across each channel of a gap junction consisting of a central hexagon surrounded by k annuli of hexagons, $0 \le k \le 25$. Fig. 5 *A* shows how the resulting $\Delta V_{channels}$ decreases with the gap junction diameter. For the largest gap junc-

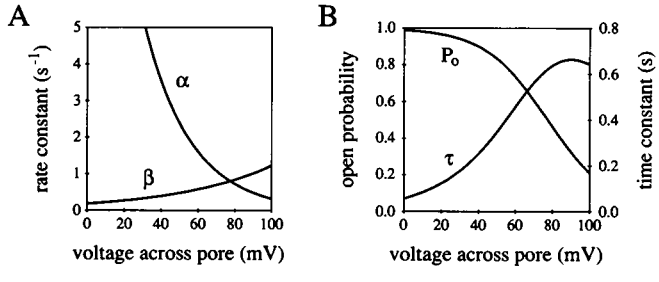

FIGURE 4 Kinetics of an individual gap junction channel. (*A*) Opening rate, α, and closing rate, β, as a function of the voltage across the channel. Curves drawn according to Eqs. 12 and 13. (*B*) Time constant, τ, and open probability, P_o, as a function of the voltage across the channel. Note different ordinate scales. Curves drawn according to $\tau = 1/(\alpha + \beta)$ and $P_o = \alpha/(\alpha + \beta)$.

TABLE 1 **Resistance of patch pipettes used in double whole cell voltage clamp experiments**

	Pipette resistance	
	In bath	On cell
	MΩ	MΩ
Weingart (1986)	1.19 ± 0.03*	1.98 ± 0.08*
Veenstra and DeHaan (1988)	2–6	5–15
Rook et al. (1988)	5–15	20–60
Burt and Spray (1988)	5–10	—
Rüdisüli and Weingart (1989)	1.5–2.5	—
Rook et al. (1990)	5–15	20–100
Veenstra (1991*b*)	4–6	10–34
Takens-Kwak et al. (1992)	5–15	15–60

* Mean ± SEM, n = 10.

tion shown, comprising 1,951 channels according to Eq. 1, $\Delta V_{channels}$ amounts to 56% of the applied voltage in the ideal case of complete compensation of the pipette series resistance. This figure is reduced to 36% (27%) if 5-MΩ (10-MΩ) pipettes are used. A gap junction comprising 1,951 channels takes up a junctional area of 0.15 μm^2, a moderate value taking into account that the surface area of gap junctions in adult rat ventricle was found to range between 0.014 and 7.7 μm^2 with an average of 0.427 μm^2 (Shibata and Yamamoto, 1979). So, we conclude from Fig. 5 *A* that cytoplasmic access resistance may give rise to large errors. We did not compute $\Delta V_{channels}$ for $N >$ 1,951, because of the large amounts of computer storage and processor time involved; the time required to solve the $N \times N$ system of linear equations defined by Eq. 9 is approximately proportional to N^3.

The actual voltage across the junctional channels decreases with increasing gap junction size (Fig. 5 *A*). As a consequence, junctional current is not simply proportional to the number of channels comprised in the gap junction. This, of course, applies to junctional conductance as well. Fig. 5 *B* depicts the (instantaneous) junctional conductance as a function of the number of channels. The dashed line shows the "expected junctional conductance," which was obtained by multiplying the number of channels by the single channel conductance of ~46 pS. The number of channels may be largely underestimated if it is estimated from the (instantaneous) junctional conductance in the usual way, i.e., by dividing it by the single channel conductance. Fig. 5 *B* does not provide an easy way to correct for cytoplasmic access resistance, because, generally, it is not known whether all channels are arranged in one large array. If, e.g., 10- to 15-MΩ pipettes are used, a conductance of ~20 nS may result from one large gap junction comprising ~1,800 channels as well as from four distinct gap junctions, each comprising ~150 channels.

The nonlinearity in the relation between junctional conductance and the number of channels may explain discrepancies between experimentally observed values of single channel conductances and open probabilities and values estimated from experiments on large gap junctions, as illustrated by the following example. Weingart (1986) observed an average junctional resistance of 3.4 MΩ (Table 1) or 1.7 MΩ after correction for pipette series resistance. Using the latter value and estimating the number of channels from ultrastructural data to be 62,000, he obtained a single channel conductance of 9.5 pS, far less than the experimentally observed value of ~50 pS. To explain this, Rüdisüli and Weingart (1991) hypothesized that the single channel open probability is ~0.2 at any transjunctional voltage ≤ 50 mV. Data on single channel open and closed times (Rook et al., 1988) as well as experimentally observed correlations between gap junctional area and junctional conductance (Rook et al., 1990), on the other hand, show that this probability is close to 1. From Fig. 5 *B*, it is likely that 62,000 junctional channels may yield a junctional resistance as high as 1.7 MΩ, if their single channel conductance is ~50 pS and their open probability is 1.

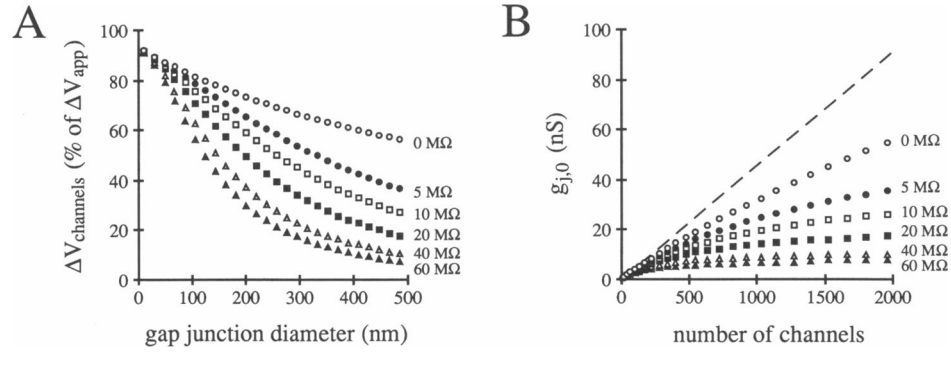

FIGURE 5 Experimental errors increase with gap junction size. (*A*) Voltage across the junctional channels, $\Delta V_{channels}$, in percents of the applied voltage, ΔV_{app}, as a function of the gap junction diameter. The resistance of each pipette is 0 MΩ (○), 5 MΩ (●), 10 MΩ (□), 20 MΩ (■), 40 MΩ (△) or 60 MΩ (▲). (*B*) Instantaneous junctional conductance, $g_{j,0}$, as a function of the number of channels comprised in the gap junction. The dashed line represents the case of negligible cytoplasmic access resistance. Symbols as in *A*.

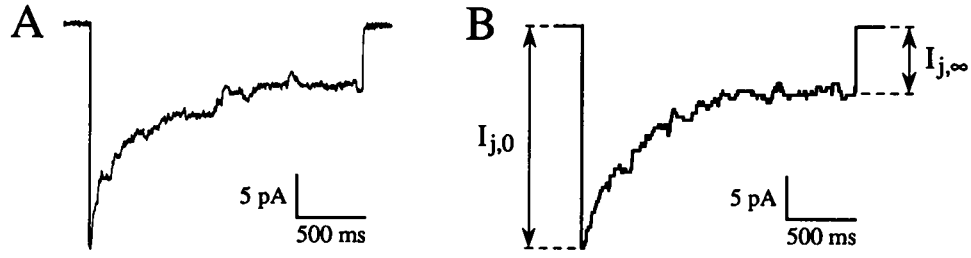

FIGURE 6 Transjunctional voltage dependence of a gap junction comprising six channels; average of 10 successive junctional current traces in response to a 100-mV, 2-s step in applied voltage. (*A*) Experimental result from a newly formed pair of neonatal rat heart cells. (*B*) Model result. R_{pip} = 30 MΩ. The instantaneous (steady-state) junctional current is $I_{j,0}$ ($I_{j,\infty}$).

Normalized steady-state junctional conductance

In experiments on small gap junctions, junctional current diminishes during voltage clamp steps if the applied voltage is large, reaching a quasi-steady-state value within 1–2 s (Fig. 6 *A*). In the experiment presented in Fig. 6 *A*, this value was ~27% of the instantaneous value. Fig. 6 *B* depicts the model counterpart of this experiment. Instantaneous junctional current, $I_{j,0}$, and (quasi) steady-state junctional current, $I_{j,\infty}$, were calculated to be 26.4 and 7.2 pA, respectively. According to Eq. 18, normalized steady-state junctional conductance amounts to 0.27, which is approximately equal to the constant average value around which the fraction of open channels is expected to fluctuate (cf. Fig. 4 *B*). In large gap junctions, however, $G_{j,\infty}$ may be considerably larger than the fraction of open channels due to an increase in $\Delta V_{channels}$ during the voltage clamp step, which, in turn, is due to (*a*) a decrease in cytoplasmic access resistance due to the decrease in the number of open channels and (*b*) a decrease in potential drop across the pipettes due to the decrease in junctional current.

To investigate the effects of gap junction size and pipette series resistance on $G_{j,\infty}$, we calculated $I_{j,0}$ and $I_{j,\infty}$ at applied voltages up to 100 mV for gap junctions where the central hexagon was surrounded by another two, five, or seven annuli of hexagons (cf. Fig. 1 *B*), the number of channels being 19, 91, and 169, respectively. We restricted our calculations to relatively small N, because the computer time involved is approximately proportional to N^4; the time required to solve the system defined by Eq. 9 is approximately proportional to N^3, and this system has to be solved repeatedly, i.e., after each channel opening or closure, the number of which is proportional to N. The calculation of a current trace in response to a 2-s step in applied voltage requires ~8 min of processor time on a VAX 4000-300 computer if N = 169. So, a similar calculation for N = 1,951 would require ~100 d of processor time. The resulting current-voltage relationships are shown in Fig. 7, *A–C*, for pipette series resistances of 0, 10, and 40 MΩ, respectively.

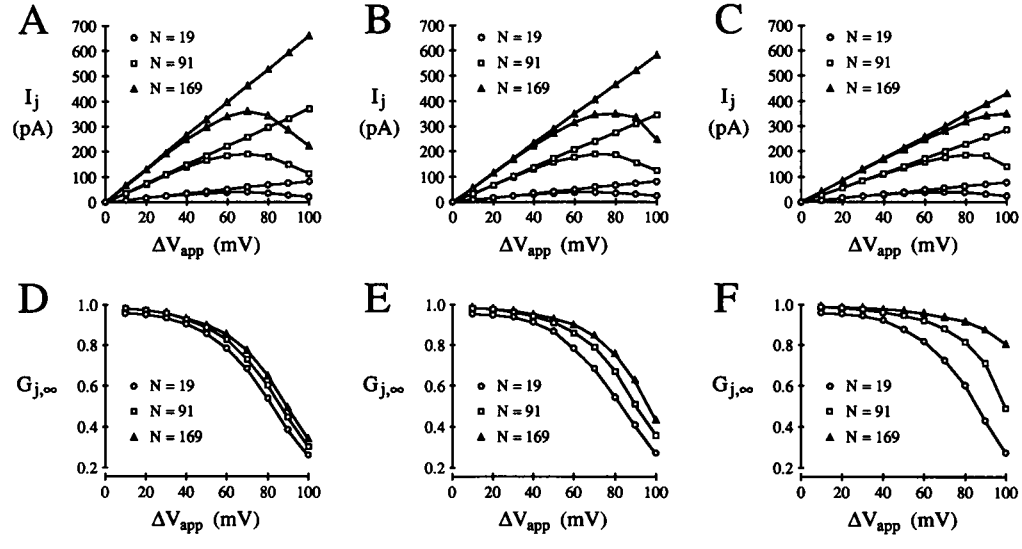

FIGURE 7 Instantaneous junctional current, $I_{j,0}$, steady-state junctional current, $I_{j,\infty}$, and the resulting normalized steady-state junctional conductance, $G_{j,\infty}$, as a function of the applied voltage, ΔV_{app}. $I_{j,0}$ and $I_{j,\infty}$ appear as straight lines and curved lines, respectively. Calculations were performed for three differently sized gap junctions, comprising 19 (○), 91 (□), and 169 (△) channels. (*A* and *D*) R_{pip} = 0 MΩ. (*B* and *E*) R_{pip} = 10 MΩ. (*C* and *F*) R_{pip} = 40 MΩ.

Of course, $I_{j,0}$ decreases with increasing R_{pip}. For $N = 19$, this decrease, from 83 pA at 0 MΩ to 78 pA at 40 MΩ, is negligible, but for $N = 169$ it is not, $I_{j,0}$ being 659 at 0 MΩ and 431 pA at 40 MΩ. At the same time, $I_{j,\infty}$ varies in a more complex way. At the highest voltage applied, it even increases with increasing R_{pip}: from 224 pA at 0 MΩ to 348 pA at 40 MΩ for $N = 169$.

The instantaneous and steady-state current-voltage relationships were combined, by means of Eq. 18, in the $G_{j,\infty}$-voltage relationships depicted in Fig. 7, *D–F*. The true effect of cytoplasmic access resistance can be inferred from Fig. 7 *D*, where $R_{pip} = 0$. At an applied voltage of 100 mV, $G_{j,\infty}$ is 0.27 for $N = 19$, 0.31 for $N = 91$, and 0.35 for $N = 169$. At nonzero pipette series resistances, the $G_{j,\infty}$ values differ by a larger amount (Fig. 7, *E* and *F*). At $R_{pip} = 10$ MΩ and $\Delta V_{app} = 100$ mV, $G_{j,\infty}$ is 0.28 for $N = 19$, 0.36 for $N = 91$, and 0.42 for $N = 169$. At $R_{pip} = 40$ MΩ, these figures are 0.30, 0.49, and 0.81, respectively. These model results demonstrate that normalized conductance values may be strongly dependent on gap junction size, especially if (uncompensated) series resistance of the pipettes is high.

Transjunctional voltage dependence

From the open probability function (Fig. 4 *B*), it is clear that I_j will not diminish substantially during voltage clamp pulses ≤ 50 mV. This may explain all cases except one, where transjunctional voltage dependence was not at all observed (Table 2). From the model results presented in Figs. 5 and 7, it is highly unlikely that in 90- to 3,900-nS gap junctions, voltage dependence can be observed during 0.2-s voltage clamp pulses, even if applied voltage is 100 mV. This may explain the remaining case where voltage dependence was not at all observed. In two studies, however, voltage dependence was also found to be absent in much smaller gap junctions (Table 2), with conductances around 10 nS (Takens-Kwak et al., 1992) or even <10 nS (Rook et al., 1988), although voltage clamp pulses up to 100 mV, and of ≥1-s duration, were applied.

To investigate whether in the latter studies the voltage dependence of single gap junction channels may have been masked due to cytoplasmic access resistance and pipette series resistance, we calculated $G_{j,\infty}$ at $\Delta V_{app} = 100$ mV for gap junctions where the central hexagon (Fig. 1 *B*) was surrounded by another 0–10 annuli of hexagons and R_{pip} ranged from 0 to 60 MΩ. The resulting $G_{j,\infty}$ values are depicted as a function of apparent (instantaneous) junctional conductance in Fig. 8. Values near 1, indicating "absence" of voltage dependence, are easily attained. For the largest gap junction shown, comprising 331 channels, $g_{j,0}$ and $G_{j,\infty}$ amount to 6.2 nS and 0.95, respectively, at $R_{pip} = 20$ MΩ. At $R_{pip} = 60$ MΩ, these figures are 4.9 nS and 0.98, respectively. This may explain that Rook et al. (1988) found "no indications of voltage-dependent decay" in the experiment shown in their Fig. 3: junctional conductance was ~6 nS and pipette resistances were ~50 MΩ.

In Fig. 3 of a more recent paper, Rook et al. (1990) demonstrated that a gap junction between neonatal rat heart cells with a conductance as low as 1.9 nS may not show voltage dependence at applied voltages up to 100 mV of 1-s duration. At first sight, this cannot be explained by our model results (Fig. 8), even if one takes into account that, due to clamping problems, $I_{j,0}$ was not well defined. It should, however, be noted that (*a*) I_j does not always reach a quasi-steady-state value within 1 s, so that normalized conductance after 1 s, denoted by $G_{j,1}$, may be considerably larger than $G_{j,\infty}$; (*b*) widely different $G_{j,1}$ values may be observed in subsequent current records if gap junctions are small, due to the stochastic nature of channel kinetics; and (*c*) pipette resistances

TABLE 2 Conductance and transjunctional voltage dependence of gap junctions between mammalian cardiac myocytes

		Junctional conductance			Transjunctional voltage dependence		
	Preparation	Range	Mean	*n*	Voltage range tested	Pulse duration	Voltage dependence observed
		nS	*nS*		*mV*	*s*	
Kameyama (1983)	Guinea pig ventricle	90–3,200	700	47	≤7	0.1	No
White et al. (1984, 1985)	Adult rat ventricle	5–100	9.9	41	≤50	2	No
Metzger and Weingart (1985)	Adult rat ventricle	—	472	114	≤10	0.2	No
Weingart (1986)	Adult rat ventricle	173–465	292	17	≤50	≤10	No
Noma and Tsuboi (1987)	Guinea pig ventricle	90–3,900	—	98	≤100	0.2	No
Maurer and Weingart (1987)	Adult guinea pig ventricle	180–400	250	13	≤50	0.2	No
Maurer and Weingart (1987)	Adult rat ventricle	100–800	200	13	≤50	0.2	No
Rook et al. (1988)	Neonatal rat	0.05–13	—	—	≤100	2	Yes*
Burt and Spray (1988)	Neonatal rat	0.05–35	13	55	≤10	2	No
Veenstra (1991*a*)	Neonatal hamster	1.5–3.0	—	2	≤100	2	Yes
Takens-Kwak et al. (1992)	Neonatal rat	0.2–20	9.4	29	≤100	1	Yes*

* Voltage dependence was observed only if junctional conductance was low.

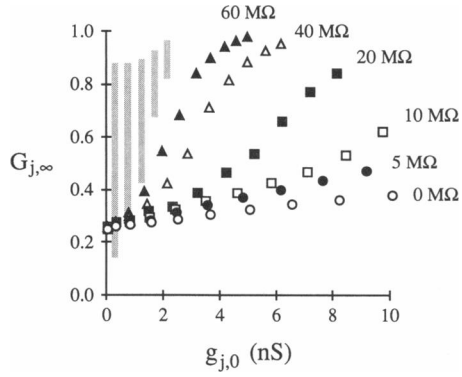

FIGURE 8 Normalized steady-state junctional conductance, $G_{j,\infty}$, at an applied voltage of 100 mV, as a function of the instantaneous junctional conductance, $g_{j,0}$. The resistance of each pipette is 0 MΩ (○), 5 MΩ (●), 10 MΩ (□), 20 MΩ (■), 40 MΩ (△), or 60 MΩ (▲). The grey bars indicate the range of normalized junctional conductance values at the end of a 100-mV, 1-s step in applied voltage, obtained from 100 current traces, the resistance of each pipette being 100 MΩ.

were ~100 MΩ. Therefore, we calculated $G_{j,1}$ values from 100 current records at ΔV_{app} = 100 mV and R_{pip} = 100 MΩ. The range of $G_{j,1}$ values obtained is indicated in Fig. 8 by grey bars, showing that also in this particular experiment voltage dependence may have been masked.

According to model results with R_{pip} = 0 (Figs. 7, *A* and *D*, and 8), large gap junctions are less sensitive to transjunctional voltage due to their high cytoplasmic access resistance, which is a natural consequence of the close packing of gap junction channels. This "disappearance of voltage dependence," however, is not as dramatic as it seemed in the experiments of Rook et al. (1988, 1990), where pipette series resistance was high (Table 1). The influence of pipette series resistance is demonstrated directly in Fig. 9 *A*, which shows the effect of a reduction in pipette resistance on the apparent transjunctional voltage dependence of a gap junction with an apparent junctional conductance of ~6.5 nS. Two current traces in response to 100 mV, 1-s voltage clamp steps were recorded from the same cell pair, one before and another after 50% series resistance compensation was used. Without series resistance compensation, voltage dependence is almost completely masked. The model counterpart, presented in Fig. 9 *B*, yields a similar result: the voltage dependence of a gap junction comprising 300 channels becomes unmasked if R_{pip} is lowered from 30 to 15 MΩ. The model current trace calculated with R_{pip} = 0 shows that the gap junction is steeply voltage dependent and that its actual conductance is 11 nS. Note that, as in Figs. 7 and 8, nonzero pipette resistances lead to an underestimation of the instantaneous junctional current and an overestimation of the normalized steady-state conductance.

Boltzmann fits

The common method to evaluate transjunctional voltage dependence of gap junction channels is to fit experimentally observed $G_{j,\infty}$-ΔV_{app} relationships to the Boltzmann relation

$$G_{j,\infty} = G_{min} + (1 - G_{min})/\{1 + \exp[A(\Delta V_{app} - V_0)]\}, \quad (19)$$

where G_{min} is the minimum $G_{j,\infty}$ attained, A expresses the steepness of the relationship, and V_0 is applied voltage where $G_{j,\infty}$ = 0.5. Theoretically, the parameters A and V_0 should equal $A_\alpha + A_\beta$ and ΔV_0, respectively, whereas the "residual conductance" G_{min} reflects some parallel voltage-insensitive "leakage-component" (Harris et al., 1981).

Veenstra (1991*b*) reported developmental changes in transjunctional voltage dependence in embryonic chick heart gap junctions, using Boltzmann fits to quantify these changes. The parameters A and V_0 of the Boltzmann fits for the 4- and 14-d cell pairs are listed in Table 3. The developmental decrease in transjunctional voltage dependence may be explained by the hypothesis that connexin45 gives way to connexin42 as the predominant connexin in the developing chick heart, resulting in a developmental increase in the relative amount of junctional channels formed by connexin42, which are less sensitive to transjunctional voltage (Veenstra et al.,

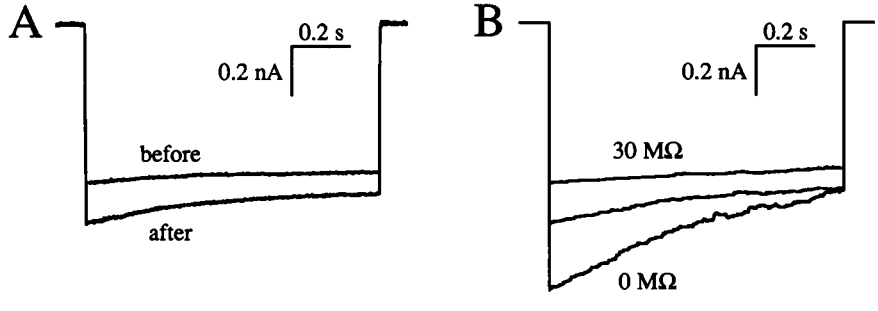

FIGURE 9 Transjunctional voltage dependence is masked by pipette series resistance; effect of a 50% reduction in pipette series resistance on junctional current in response to a 100-mV, 1-s step in applied voltage. (*A*) Experimental result from a pair of neonatal rat heart cells; junctional current traces before and after 50% series resistance compensation were used. Uncompensated pipette resistances were 25 and 35 MΩ. (*B*) Model result, the gap junction comprising 300 channels; junctional current traces with R_{pip} = 30 MΩ and R_{pip} = 15 MΩ. Junctional current in the ideal case of complete compensation of pipette series resistance is also shown.

TABLE 3 Junctional conductance and parameters of the Boltzmann relation

	$g_{j,0}$	G_{min}	A	V_0
	nS		mV^{-1}	mV
Experiment				
4-d	2.19 ± 0.48*	0.18	0.058	42
14-d	6.59 ± 2.19*	0.28	0.096	50
Model				
Low g_j	2.14	0.19	0.056	44
High g_j	6.69	0.24	0.075	52

* Mean ± SEM, n = 8.

1991). Junctional conductance, however, changed with development as well (Table 3). Figs. 7 and 8 make clear that gap junctions of different size may exhibit largely different $G_{j,\infty}$-ΔV_{app} relationships, although the individual channels are equally sensitive to the voltage across them. So, we wondered to which extent the developmental changes in gap junction size might have led to the observed differences in A and V_0, if connexin42 were the predominant connexin in both 4- and 14-d cell pairs. We changed some parameters of our model to make it applicable to embryonic chick heart gap junctions. First, we set R_{pip} to 20 MΩ, because (uncompensated) pipette series resistance was 19.8 ± 0.8 MΩ (mean ± SEM, n = 48). Second, we set γ to 160 pS, in agreement with the experimentally observed single channel conductance (Veenstra et al., 1991). With r_c = 1.0 nm, A_α = 0.018 mV^{-1}, A_β = 0.036 mV^{-1}, λ = 1.0 s^{-1}, and ΔV_0 = 40 mV, we obtained current traces similar to those of Veenstra (1991*b*) (not shown). We performed calculations with N = 17 and N = 71 to mimic the average conductance of 4- and 14-d cell pairs (Table 3). The resulting $G_{j,\infty}$-ΔV_{app} relationships were fitted to Eq. 19 in the same way as Veenstra's experimental data. The thus obtained values of the parameters of the Boltzmann relation are presented in Table 3 and are quite close to those of Veenstra (1991*b*). This, again, demonstrates that one has to be careful in drawing conclusions from the parameters of Boltzmann fits.

It has been hypothesized that nonzero G_{min} values originate from a separate class of voltage-insensitive channels, i.e., channels that do not close in response to large transjunctional voltages (Spray et al., 1981; Veenstra, 1990; Rook, 1991). In our model, the residual conductance is a direct consequence of the nonzero single channel open probability at large voltages (Fig. 4 *B*), thus providing an alternative explanation for the >0.2 G_{min} values observed in experiments on pairs of mammalian cardiac myocytes (Rook et al., 1988; Veenstra, 1991*a*) and transfectants expressing connexin43 (Fishman et al., 1991). It may also explain why this "residual conductance" increases with gap junction size, as may be inferred from Fig. 9 of Takens-Kwak et al. (1992).

Optimum experimental conditions

The model results presented above can be used to define the experimental conditions under which the dual voltage clamp method may be used for analysis of gap junction channel properties. First, as pointed out before, the effect of nonjunctional membrane current must be negligible. If, in addition, (uncompensated) pipette series resistance is low, then meaningful information about gap junction channel properties may be obtained from small gap junctions where the effects of cytoplasmic access resistance are negligible. To assure, e.g., that the errors in normalized conductance values, i.e., the deviations from theoretical values, are <15%, apparent junctional conductance must be <6 nS (<4 nS) if pipette series resistance is 5 MΩ (10 MΩ).

Model assumptions

Model results resemble experimental results to a very reasonable degree (Figs. 6 and 9). It should be kept in mind, however, that several fundamental assumptions were made in constructing the model. Besides, given the model, several guesses had to be made in assigning values to model parameters. One fundamental assumption is that all junctional channels are open at the beginning of a voltage clamp step, thus maximizing the effects of cytoplasmic access resistance. There are, indeed, experimental results supporting this assumption (Rook et al., 1988, 1990).

Another fundamental assumption is that the gap junction channel has a right cylindrical shape. The cytoplasmic potential drop increases with increasing channel diameter and decreasing channel length (not shown), suggesting that the effect of cytoplasmic access resistance are stronger if the channel conforms more closely to, e.g., the shape of two abutting cones with their wide mouths facing the cytoplasm.

We thank Dr. A. van Oosterom, Laboratory of Medical Physics and Biophysics, Katholieke Universiteit Nijmegen, The Netherlands, for helping us to form the cytoplasmic access resistance equations, and Dr. B. R. Takens-Kwak for providing us with experimental data.

This study was supported by the Netherlands Organization for Scientific Research (NWO) through the Foundation for Biophysics.

Received for publication 6 February 1992 and in final form 9 June 1992.

REFERENCES

Burt, J. M., and D. C. Spray. 1988. Single-channel events and gating behavior of the cardiac gap junction channel. *Proc. Natl. Acad. Sci. USA.* 85:3431–3434.

Chanson, M., R. Bruzzone, D. C. Spray, R. Regazzi, and P. Meda. 1988. Cell uncoupling and protein kinase C: correlation in a cell line but not in a differentiated tissue. *Am. J. Physiol.* 255:C699–C704.

Chapman, R. A., and C. H. Fry. 1978. An analysis of the properties of frog ventricular myocardium. *J. Physiol. (Lond.).* 283:263–282.

Clay, J. R., and L. J. DeFelice, 1983. Relationship between membrane excitability and single channel open-close kinetics. *Biophys. J.* 42:151–157.

Colquhoun, D., and A. G. Hawkes. 1983. The principles of the stochastic interpretation of ion-channel mechanisms. *In* Single-Channel Recording. B. Sakmann and E. Neher, editors. Plenum Publishing Corp., New York. 135–175.

de Mazière, A. M. G. L., A. C. G. van Ginneken, R. Wilders, H. J. Jongsma, and L. N. Bouman. 1992. Spatial and functional relationship between myocytes and fibroblasts in the rabbit sinoatrial node. *J. Mol. Cell. Cardiol.* 24:567–578.

Fishman, G. I., A. P. Moreno, D. C. Spray, and L. A. Leinwand. 1991. Functional analysis of human cardiac gap junction channel mutants. *Proc. Natl. Acad. Sci. USA.* 88:3525–3529.

Forsythe, G. E., and W. R. Wasow. 1960. Finite-Difference Methods for Partial Differential Equations. John Wiley & Sons Inc., New York. 444 pp.

Giaume, C. 1991. Application of the patch-clamp technique to the study of junctional conductance. *In* Biophysics of Gap Junction Channels. C. Peracchia, editor. CRC Press, Inc., Boca Raton, FL. 175–190.

Hall, J. E. 1975. Access resistance of a small circular pore. *J. Gen. Physiol.* 66:531–532.

Harris, A. L., D. C. Spray, and M. V. L. Bennett. 1981. Kinetic properties of a voltage-dependent junctional conductance. *J. Gen. Physiol.* 77:95–117.

Hille, B. 1968. Drugs and sodium channels of nerve. *J. Gen. Physiol.* 51:199–219.

Hille, B. 1984. Ionic Channels of Excitable Membranes. Sinauer, Sunderland, MA. 426 pp.

Jongsma, H. J., and R. Wilders. 1992. Voltage dependence of gap junction conductance is masked by a voltage drop across the cytoplasm and the recording pipettes. *Biophys. J.* 61:409a. (Abstr.)

Jongsma, H. J., R. Wilders, and M. B. Rook. 1990. Modulation of gap junction conductance by transcellular electrical fields. *Biophys. J.* 57:246*a*. (Abstr.)

Jongsma, H. J., R. Wilders, A. C. G. van Ginneken, and M. B. Rook. 1991. Modulatory effect of the transcellular electrical field on gap junction conductance. *In* Biophysics of Gap Junction Channels. C. Peracchia, editor. CRC Press, Inc., Boca Raton, FL. 163–172.

Kameyama, M. 1983. Electrical coupling between ventricular paired cells isolated from guinea-pig heart. *J. Physiol. (Lond.).* 366:177–195.

Makowski, L., D. L. D. Caspar, W. C. Phillips, T. S. Baker, and D. A. Goodenough. 1984. Gap junction structures VI: variation and conservation in connexon conformation and packing. *Biophys. J.* 45:208–218.

Manjunath, C. K., and E. Page. 1985. Cell biology and protein composition of cardiac gap junctions. *Am. J. Physiol.* 248:H783–H791.

Maurer, P., and R. Weingart. 1987. Cell pairs isolated from adult guinea-pig and rat hearts: effects of $[Ca^{2+}]_i$ on nexal membrane resistance. *Pfluegers Arch. Eur. J. Physiol.* 409:394–402.

Metzger, P., and R. Weingart. 1985. Electric current flow in cell pairs isolated from adult rat hearts. *J. Physiol. (Lond.).* 366:177–195.

Moreno, A. P., A. C. Campos de Carvalho, V. Verselis, B. Eghbali, and D. C. Spray. 1991*a*. Voltage-dependent gap junction channels are formed by connexin32, the major gap junction protein of rat liver. *Biophys. J.* 59:920–925.

Moreno, A. P., B. Eghbali, and D. C. Spray. 1991*b*. Connexin32 gap junction channels in stably transfected cells: equilibrium and kinetic properties. *Biophys. J.* 60:1267–1277.

Neyton, J., and A. Trautmann. 1985. Single-channel currents of an intercellular junction. *Nature (Lond.).* 317:331–335.

Noma, A., and N. Tsuboi. 1987. Dependence of junctional conductance on proton, calcium and magnesium ions in cardiac paired cells of guinea-pig. *J. Physiol. (Lond.).* 382:193–211.

Revel, J. P., and M. J. Karnovsky. 1967. Hexagonal array of subunits in intercellular junctions of the mouse heart and liver. *J. Cell Biol.* 33:C7–C12.

Rook, M. B. 1991. Gap junctions between heart cells in vitro: electrophysiological, ultrastructural, and immunocytochemical correlates. Ph.D. Thesis. University of Amsterdam. 129 pp.

Rook, M. B., H. J. Jongsma, and A. C. G. van Ginneken. 1988. Properties of single gap junctional channels between isolated neonatal rat heart cells. *Am. J. Physiol.* 255:H770–H782.

Rook, M. B., B. de Jonge, H. J. Jongsma, and M. A. Masson-Pévet. 1990. Gap junction formation and functional interaction between neonatal rat cardiocytes in culture: a correlative physiological and ultrastructural study. *J. Membr. Biol.* 118:179–192.

Rüdisüli, A., and R. Weingart. 1989. Electrical properties of gap junction channels in guinea-pig ventricular cell pairs revealed by exposure to heptanol. *Pfluegers Arch. Eur. J. Physiol.* 415:12–21.

Rüdisüli, A., and R. Weingart. 1991. Gap junctions in adult ventricular muscle. *In* Biophysics of Gap Junction Channels. C. Peracchia, editor. CRC Press, Inc., Boca Raton, FL. 43–56.

Schwarzmann, G., H. Wiegandt, B. Rose, A. Zimmerman, D. Ben-Haim, and W. R. Loewenstein. 1981. Diameter of the cell-to-cell junctional membrane channels as probed with neutral molecules. *Science (Wash. DC).* 213:549–551.

Shibata, Y., and T. Yamamoto. 1979. Freeze-fracture studies of gap junctions in vertebrate cardiac muscle cells. *J. Ultrastruct. Res.* 67:79–88.

Spray, D. C., and J. M. Burt. 1990. Structure-activity relations of the cardiac gap junction channel. *Am. J. Physiol.* 258:C195–C205.

Spray, D. C., A. L. Harris, and M. V. L. Bennett. 1981. Equilibrium properties of a voltage-dependent junctional conductance. *J. Gen. Physiol.* 77:77–93.

Takens-Kwak, B. R., H. J. Jongsma, M. B. Rook, and A. C. G. van Ginneken. 1992. Mechanism of heptanol-induced uncoupling of cardiac gap junctions: a perforated-patch clamp study. *Am. J. Physiol.* 262:C1531–C1538.

Veenstra, R. D. 1990. Voltage-dependent gating of gap junction channels in embryonic chick ventricular cell pairs. *Am. J. Physiol.* 258:C662–C672.

Veenstra, R. D. 1991*a*. Comparative physiology of cardiac gap junction channels. *In* Biophysics of Gap Junction Channels. C. Peracchia, editor. CRC Press, Inc., Boca Raton, FL. 131–144.

Veenstra, R. D. 1991*b*. Developmental changes in regulation of embryonic chick heart gap junctions. *J. Membr. Biol.* 119:253–265.

Veenstra, R. D., and R. L. DeHaan. 1988. Cardiac gap junction channel activity in embryonic chick ventricular cells. *Am. J. Physiol.* 254:H170–H180.

Veenstra, R. D., H. Z. Wang, E. M. Westphale, and E. C. Beyer. 1991. Functional differences between embryonic chick heart connexins. *J. Cell Biol.* 115:191*a*. (Abstr.)

Weingart, R. 1986. Electrical properties of the nexal membrane studied in rat ventricular cell pairs. *J. Physiol. (Lond.).* 370:267–284.

White, R. L., D. C. Spray, G. J. Schwartz, B. A. Wittenberg, and M. V. L. Bennett. 1984. Some physiological and pharmacological properties of gap junctions. *Biophys. J.* 45:279*a*. (Abstr.)

White, R. L., D. C. Spray, A. C. Campos de Carvalho, B. A. Wittenberg, and M. V. L. Bennett. 1985. Some electrical and pharmacological properties of gap junctions between adult ventricular myocytes. *Am. J. Physiol.* 249:C447–C455.

Wittenberg, B. A., R. L. White, R. D. Ginzberg, and D. C. Spray. 1986. Effect of calcium on the dissociation of the mature rat heart into individual and paired myocytes: electrical properties of cell pairs. *Circ. Res.* 59:143–150.

Zampighi, G., and P. N. T. Unwin. 1979. Two forms of isolated gap junctions. *J. Mol. Biol.* 135:451–464.